END-TO-END CALIBRATION PATTERNS DESIGN TO ESTIMATE THE POINT SPREAD FUNCTION FOR A SHIFT VARIANT OPTICAL SYSTEM

SEBASTIAN CAMPO CRUZ

UNIVERSIDAD INDUSTRIAL DE SANTANDER
FACULTAD DE INGENIERÍAS FISICOMECÁNICAS
ESCUELA DE INGENIERÍA ELÉCTRICA, ELECTRÓNICA Y TELECOMUNICACIONES
BUCARAMANGA
2024

END-TO-END CALIBRATION PATTERNS DESIGN TO ESTIMATE THE POINT SPREAD FUNCTION FOR A SHIFT VARIANT OPTICAL SYSTEM

SEBASTIAN CAMPO CRUZ

Degree work presented as a requirement to qualify for the title of Electronic Engineer

Advisor:
ING. KAREN ANDREA FONSECA ESTUPIÑAN.

Co-Advisor:
PhD. HENRY ARGUELLO FUENTES
Co-Advisor:
PhD. HANS YECID GARCIA ARENAS

UNIVERSIDAD INDUSTRIAL DE SANTANDER
FACULTAD DE INGENIERÍAS FISICOMECÁNICAS
ESCUELA DE INGENIERÍA ELÉCTRICA, ELECTRÓNICA Y TELECOMUNICACIONES
BUCARAMANGA
2024

ACKNOWLEDGEMENTS

I would like to express my deep gratitude to several people who have been fundamental in my academic and personal journey.

First and foremost, I thank my parents for their unwavering support, inspiration, and hope throughout this academic journey. Their belief in me has been a cornerstone of my success.

I am also deeply grateful to my family, who have believed in me and inspired me every single day since I started this career. Their constant encouragement has been invaluable.

I extend my deepest thanks to my friends Jorge, Angie, Valeria, Nubia, Carlos, Melissa, and Angel. Your unwavering support, willingness to help without hesitation, and refusal to let me give up have been a source of great strength and happiness in my life. Thank you for being so real.

Finally, I am immensely grateful to the High Dimensional Signal Processing investigation group for their help, guidance, and contributions to my personal and professional growth. Special thanks to Professor Henry for this priceless opportunity and guidance, to Professor Hans for his invaluable assistance and encouragement, and to my dear friend, Karen, whose belief in me and support made all of this possible.

Dedicated to those who believed and made me believe.

TABLE OF CONTENTS

LIST OF FIGURES

Page.

RESUMEN

TÍTULO: DISEÑO DE PATRONES DE CALIBRACIÓN PARA ESTIMAR LA FUNCIÓN DE DISPERSIÓN DE PUNTO DE UN SISTEMA ÓPTICO VARIANTE USANDO ALGORITMOS DE APRENDIZAJE PROFUNDO DE EXTREMO A EXTREMO. *

AUTOR: SEBASTIAN CAMPO CRUZ **

PALABRAS CLAVE: FUNCIÓN DE DISPERSIÓN DE PUNTO, SISTEMAS ÓPTICOS, ELEMENTOS ÓPTICOS DIFRACTIVOS, ANÁLISIS DE COMPONENTES PRINCIPALES, PATRONES DE CALIBRACIÓN.

DESCRIPCIÓN:

La adquisición de imágenes espectrales depende de la implementación de sistemas ópticos; algunos de ellos como los sistemas ópticos variantes, requieren un proceso de calibración en donde la función de dispersión de punto es adquirida en todas las coordenadas espaciales del sistema. Conocer la función de dispersión de punto es esencial ya que permite obtener una descripción completa del comportamiento del sistema a través de la dimensión espacial y espectral, facilitando procesos como la reconstrucción computacional de imágenes espectrales, decodificación de imágenes, entre otros. Adquirir la función de dispersión de punto en todas las coordenadas espaciales del sistema es una tarea compleja y que consume bastante tiempo ya que requiere un número elevado de capturas en donde cada una tiene un tiempo de integración elevado. Por estas razones, este trabajo propone un método para obtener una aproximación de la función de dispersión de punto de un sistema óptico variante mediante la captura de un conjunto de patrones de calibración diseñados usando análisis de componentes principales. Los resultados de simulación muestran que utilizando un 84% menos capturas, es posible obtener una aproximación de la función de dispersión de punto con un pico de relación señal a ruido promedio de 40 db y un índice de similaridad estructural de 90%. Resultados de implementación mostraron un pico de relación señal a ruido promedio de 40 db y un índice de similaridad estructural promedio de 71%.

---

* Trabajo de Grado

** Facultad de Ingenierías Físico-Mecánicas. Escuela de Ingenierías Eléctrica, Electrónica y de Telecomunicaciones.
Directora: Ing. KAREN ANDREA FONSECA ESTUPIÑAN.

ABSTRACT

TITLE: END-TO-END CALIBRATION PATTERNS DESIGN TO ESTIMATE THE POINT SPREAD FUNCTION FOR A SHIFT VARIANT OPTICAL SYSTEM [*]

AUTHOR: SEBASTIAN CAMPO CRUZ [**]

KEYWORDS: POINT-SPREAD-FUNCTION, OPTICAL SYSTEMS, DIFFRACTIVE OPTICAL ELEMENTS, PRINCIPAL COMPONENT ANALYSIS, CALIBRATION PATTERNS.

DESCRIPTION:

Spectral image (SI) acquisition relies on optical systems implementation; some systems as the shift-variant, require a calibration process where the point spread function (PSF) is acquired at each spatial point. Knowing the PSF is essential as it allows a complete description of the system behavior through the spatial and spectral dimensions, facilitating process like computational spectral image (CSI) reconstruction, and reverse codification, among others. Acquiring the complete PSF of an optical system is a complex and time consuming process as it requires several snapshots, each one with high acquisition time. For these reasons, this paper proposes a method to obtain an approximation of the PSF for a shift-variant optical system by capturing a set of calibration patterns designed using principal component analysis (PCA). Simulation results showed that by using 84% fewer snapshots, it is possible to obtain a PSF with an average peak signal-to-noise ratio (PSNR) of 40 dB and an average structural similarity index measure (SSIM) of 90%. Implementation results showed an average PSNR of 40 dB and an average SSIM of 71%.

---

[*] BSc Thesis

[**] Facultad de Ingenierías Físico-Mecánicas. Escuela de Ingenierías Eléctrica, Electrónica y de Telecomunicaciones.
Directora: Eng. KAREN ANDREA FONSECA ESTUPIÑAN.

INTRODUCTION

Spectral imaging acquires and processes the electromagnetic wavefront reflected by objects in a scene; the resulting information can be represented as a 3D data cube called a spectral image (SI), where the first two dimensions correspond to the spatial information and the third dimension contains spectral information [1]. With SIs, is possible to perform tasks like the identification of materials or objects by analyzing their distinct spectral responses, which arise from their physical or chemical properties influencing absorption or reflection within specific spectral bands [1]. This technique finds applications across various fields, such as food inspection processes to ensure quality and safety standards [2], in medical settings for the analysis of pigmented skin lesions [3], and in environmental monitoring initiatives [45].

---

[1] Jorge BACCA, Emmanuel MARTINEZ, and Henry ARGUELLO. "Computational spectral imaging: a contemporary overview". In: *J. Opt. Soc. Am. A* 40.4 (Apr. 2023), pp. C115–C125. DOI: 10.1364/JOSAA.482406.

[2] Hongyi GE et al. "Applications of THz Spectral Imaging in the Detection of Agricultural Products". In: *Photonics* 8.11 (2021). DOI: 10.3390/photonics8110518.

[3] Eleni ALOUPOGIANNI et al. "Design of a Hyper-Spectral Imaging System for Gross Pathology of Pigmented Skin Lesions". In: *2021 43rd Annual International Conference of the IEEE Engineering in Medicine & Biology Society (EMBC)*. 2021, pp. 3605–3608. DOI: 10.1109/EMBC46164.2021.9629512.

[4] Martin De BIASIO et al. "UAV-based environmental monitoring using multi-spectral imaging". In: *Airborne Intelligence, Surveillance, Reconnaissance (ISR) Systems and Applications VII*. ed. by Daniel J. HENRY. Vol. 7668. International Society for Optics and Photonics. SPIE, 2010, p. 766811. DOI: 10.1117/12.864470.

[5] Mary B. STUART, Andrew J. S. MCGONIGLE, and Jon R. WILLMOTT. "Hyperspectral Imaging in Environmental Monitoring: A Review of Recent Developments and Technological Advances in Compact Field Deployable Systems". In: *Sensors* 19.14 (2019). DOI: 10.3390/s19143071.

Many advanced SI acquisition methods employ 1D or 2D sensors. Consequently, obtaining a 3D data cube directly using commercial sensors is a challenging task. Computational spectral imaging (CSI) has emerged as a sensing tool where 3D data can be obtained using 2D coded projections, therefore, to retrieve the SI, a computational recovery process must be employed using different algorithms [1]. An optical system is considered shift-variant in the spectral axis when each spectral band has a unique PSF. In addition, reconstruction via CSI completely requires to acquire the complete PSF through the spectral axis. As the shift-variant systems have a unique PSF at each spatial point [6], it must be acquired by sensing the response of the system to a point source at each spatial point in the sensor, resulting in a time-consuming process due to the number of samples that need to be captured. Due to the challenging nature of capturing the complete PSF of optical systems, most of the state-of-the-art work focuses on estimating or reducing the needed PSFs using different hardware or software techniques. PSF estimation is commonly used in tasks like removing blur from images by using blind deconvolution, also is used in to reverse applied codification with elements like colored-coded apertures [7].

The state-of-the-art has explored the use of a sensing model with a spatially shift-inveriant convolution between the unknown scene and a PSF at each spectral band [7]. To overcome the shift-variant property of the system, a periodic structure was imposed on the CCA. The resulting CCA is composed of a QxQ kernel that is repeated along the x and y axes; this way, the amount of PSFs is reduced to Q^2 compared to the N^2 PSFs originally needed, where NxN is the size of the sensor. On the other hand,

---

[6] Sergio URREA et al. “Optical Solutions for Spectral Imaging Inverse Problems with a Shift-Variant System.” In: *Proceedings of the IEEE/CVF International Conference on Computer Vision*. 2023, pp. 4157–4164.

[7] Henry ARGUELLO et al. “Shift-variant color-coded diffractive spectral imaging system”. In: *Optica* 8.11 (2021), pp. 1424–1434.

reducing the amount of PSFs needed is possible by leverage the fact that the pixels of a blurred image are more correlated in the direction of the blurring trajectory of the PSF than in other directions. [8] shows that the correlation matrix calculated for a patch of a clean image is almost a diagonal matrix, meaning that the pixels of a clean image are uncorrelated, but the pixels of a blurred image describe a higher correlation. By knowing this property, it is possible to find the PSF of the system by calculating the autocorrelation matrix from the blurred image and using phase retrieval.

In [9], they explore the use of calibration patterns to improve image quality and reduce blur. A checkerboard pattern was designed in order to improve blur detection. Checkerboard patterns are commonly used to fix lens aberrations, but the pattern itself must be in focus during calibration, making it necessary to adjust the position of the calibration pattern with respect to the sensor. The method implements software that detects the pose of the check board with respect to the camera; additionally, the check board has a specially designed pattern that can be detected in the presence of blur. This way, the system can be calibrated using a single static pattern at a fixed distance.
Therefore state-of-the-art methods allow dataset dimensionality reduction to a representation of their main characteristics. Principal component analysis is a commonly used dataset reduction technique as it enables the projection of the original data to a low-dimensional space reducing the amount of insignificant and irrelevant data [10].

---

[8] Wei HU, Jianru XUE, and Nanning ZHENG. "PSF estimation via gradient domain correlation". In: *IEEE Transactions on Image Processing* 21.1 (2011), pp. 386–392.

[9] Alexander REUTER, Hans-Peter SEIDEL, and Ivo IHRKE. "BlurTags: spatially varying PSF estimation with out-of-focus patterns". In: *20th International Conference on Computer Graphics, Visualization and Computer Vision 2012, WSCG'2012*. 2012, pp. 239–247.

[10] Nitika SHARMA and Kriti SAROHA. "A novel dimensionality reduction method for cancer dataset using PCA and Feature Ranking". In: *2015 International Conference on Advances in Computing, Communications and Informatics (ICACCI)*. 2015, pp. 2261–2264. DOI: 10.1109/ICACCI.2015.7275954.

For these reasons, this paper proposes a method to approximate the complete PSF of a shift variant optical system by capturing a set of calibration patterns designed using PCA compression. The approximation of the PSF is calculated using inverse PCA. Simuation tests showed that the designed method requires 84% less captures to obtain a reconstructed PSF with an average PSNR of 40 dB and average SSIM of 90% compared to the simulated PSF. Implementation results showed that the method requires 97.7% less captures to obtain a PSF with an average PSNR of 40 dB and average SSIM of 71% compared to the acquired PSF.

1. SHIFT-VARIANT OPTICAL SYSTEM

An optical system is considered shift-variant when the PSF presents variations depending on the position of the input light, which means that each spatial point on the system has a unique PSF. The image formation model for different optical systems consists of the convolution between an unknown scene and a PSF [7]. Some applications, like blur simulation and removal, require modeling the blur as the convolution between an image and different PSFs along the field of view due to the uneven nature of the blur of the optical system[11]. These blurs are caused by the diffraction of light through a finite aperture, which band-limits the spatial frequencies of the output image [12].

1.1. DIFFRACTIVE OPTICAL ELEMENTS

Diffractive optical elements modify the phase of incident wave light by employing an irregular height map on the lens surface. This modulation is modeled using a point spread function (PSF) at different wavelengths [7]. The resulting optical system is smaller in size and can be adjusted to enhance both coding and reconstruction processes. Modulating the phase of incident wave light increases the optical system shift-variant property, improving coding and enabling high spectral resolution. Additionally, DOEs offer the advantage of manipulating light in unconventional ways compared to conventional elements, and they can incorporate multiple functions into a single optical element.

---

[11] Loic DENIS et al. “Fast approximations of shift-variant blur”. In: *International Journal of Computer Vision* 115 (2015), pp. 253–278.

[12] Gregory M ROBBINS and Thomas S HUANG. “Inverse filtering for linear shift-variant imaging systems”. In: *Proceedings of the IEEE* 60.7 (1972), pp. 862–872.

The shift-variant property of optical systems is crucial in mitigating the ill-posed nature of the CSI inverse problem. To enhance this property, a double DOE codification has been proposed in certain studies, as discussed in [6]. This approach induces variations in both spectral and spatial domains, thereby enhancing the encoding of the captured data. This paper uses the double DOE architecture shown in figure 1, where $U(x,y)$ represents the wavefront propagated from the scene, $U(x_1,y_1)$ represents the second wavefront propagated a distance z_1 to the first DOE, $U(x_2,y_2)$ represents the wavefront propagated a distance z_2 and modulated by the first DOE that has a height map $h(x_1,y_1)$, and finally $U(x_3,y_3)$ represents the wavefront propagated to the sensor a distance z_3 and modulated by the second DOE that has a height map $h(x_2,y_2)$.

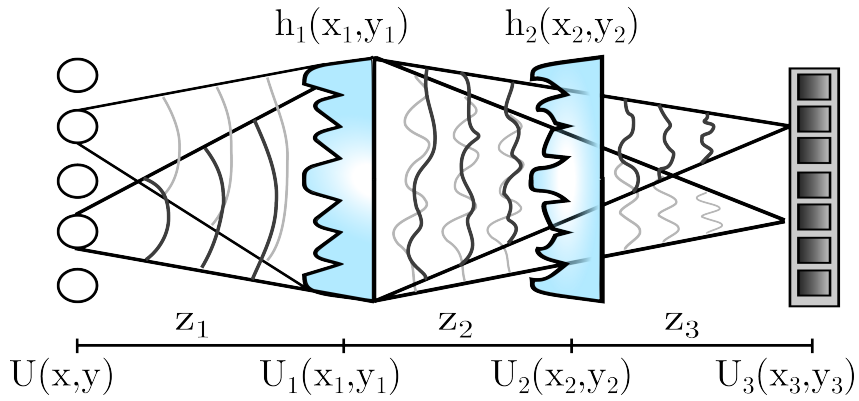

Figure 1. Double DOE architecture used.

Figure 2 illustrates the uneven surface of the DOES used through the simulation process.

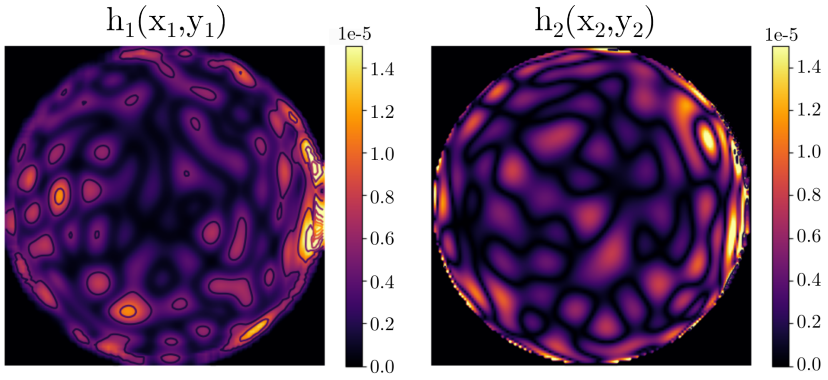

Figure 2. Illustration of the uneven surface of the DOE lenses used through the simulation process. Both DOEs have different height maps $h(x_1, y_1)$ and $h(x_2, y_2)$.

1.2. PROPAGATION MODEL

To calculate the propagation model, three operations are needed: propagation between optical elements, DOE wavefront phase codification, and sensing. Given the optical system in figure 1, the first DOE has a height map $h_1(x_1, y_1)$, and the second DOE has a height map $h_2(x_2, y_2)$. The effect of the DOE is defined by equation 1.

$$\phi(x, y, \lambda) = e^{\frac{j2\pi\Delta_{n\lambda}h(x,y)}{\lambda}} \tag{1}$$

Where $h(x, y)$ is the height map of the DOE and $\Delta_{n\lambda}$ is the diffractive index of the DOE. For this work, the propagation between optical elements is modeled by Fresnel propagation, which is an approximation of the Huygens-Fresnel principle. Given a wavefront $U(x, y, \lambda)$ propagated through air a distance z, the Fresnel operator is described in equation 2 [13].

$$P\{U(x, y, \lambda), z\} = \frac{e^{jkz}}{j\lambda z} \iint U(x', y', \lambda) e^{\frac{jk}{2z}[(x-x')^2+(y-y')^2]} \tag{2}$$

---

[13] Joseph W GOODMAN. *Introduction to Fourier optics*. Roberts and Company publishers, 2005.

Equation 2 could be rewritten using convolution, as shown in equation 3.

$$P\{U(x,y,\lambda),z\} = \frac{e^{jkz}}{j\lambda z}(U(x,y,\lambda) * e^{\frac{jk}{2z}(x^2+y^2))} \tag{3}$$

Considering the wavefront before the first DOE $U(x,y,\lambda)$, the propagation to a distance z_1 is described in equation 4.

$$U_1(x_1,y_1,\lambda) = P\{U(x,y,\lambda),z_1\} \tag{4}$$

Considering that the first DOE has a codification effect $\phi_1(x_1,y_1,\lambda)$, the propagation of the second wavefront $U_1(x_1,y_1,\lambda)$ to a distance z_2 between the DOEs is described in equation 5.

$$U_2(x_2,y_2,\lambda) = P\{\phi_1(x_1,y_1,\lambda)U_1(x_1,y_1,\lambda),z_2\} \tag{5}$$

The final wavefront propagated to the sensor at a distance of z_3 with the codification from the second DOE, $\phi_2(x_2,y_2,\lambda)$, is shown in equation 6.

$$U_3(x_3,y_3,\lambda) = P\{\phi_2(x_2,y_2,\lambda)U_2(x_2,y_2,\lambda),z_3\} \tag{6}$$

2. END-TO-END CALIBRATION PATTERNS DESIGN

The proposed method presented in figure 3 consists of modeling a compression operator $P\{\cdot\}$ as equation 7 shows:

$$\mathrm{P}\{\mathbf{Y}\} = \hat{\mathbf{Y}} = \mathbf{W}\mathbf{Y} \tag{7}$$

Where $\mathbf{W}$ is a basis matrix generated through the compression process and $\mathbf{Y}$ is the original PSF and $\hat{\mathbf{Y}}$ is the compressed PSF. Equation 8 shows the complete transformation of the PSF in order to obtain the estimated PSF.

$$\tilde{\mathbf{Y}} = (\mathbf{P^{-1}}(\mathbf{H}(\Psi_\theta(\hat{\mathbf{Y}})))) \tag{8}$$

Where $\Psi_\theta\{\cdot\}$ is the unrolling network operator, $\mathbf{H}(\cdot)$ is the optical system effect and $\mathbf{P}\{\cdot\}$ is the compression operator.

The calibration patterns could be obtained by resolving the optimization problem showed in equation 9.

$$\arg\min_\theta \mathcal{L}(\mathbf{P^{-1}}(\mathbf{H}(\Psi_\theta(\hat{\mathbf{Y}}))), \mathbf{Y}) \tag{9}$$

Equation 10 shows that for the $\mathcal{L}\{\cdot\}$ operator, an L2 norm was selected in order to obtain θ.

$$\mathcal{L}(\tilde{Y}, Y) = \|(\mathbf{P^{-1}}(\mathbf{H}(\Psi_\theta(P(\mathbf{Y})))) - \mathbf{Y})\|_2^2 \tag{10}$$

3. PRINCIPAL COMPONENT ANALYSIS

PCA is a versatile statistical method for reducing a case-by-variables data table to its essential features, called principal components. Principal components are a few linear combinations of the original variables that maximally explain the variance of all the variables [14]. Mathematically, PCA depends upon the eigen-decomposition of positive semi-definite matrices and upon the singular value decomposition (SVD) of rectangular matrices [15]. As the principal goal of this technique is to reduce the amount of information to its most representative components, PCA compression is used as the dataset reduction technique, as shown in later sections. The overall procedure to perform PCA is explained in [16]. The first step is the normalization of the raw data, as shown in equation 11.

$$\mathrm{P_{norm}} = \frac{\mathrm{P_{i,j}} - \overline{\mathrm{P}}}{\sigma_P} \tag{11}$$

Where $P_{i,j}$ is the raw data matrix, $\overline{P}$ is the mean of the P matrix, σ_P is the standard deviation of P, and X is the standardized matrix. With P_{norm}, is possible to calculate the covariance matrix of the data as shown in equation 12.

$$\Sigma = \frac{1}{\mathrm{N}} \sum_{\mathrm{i}}^{\mathrm{N}} (\mathrm{P_{norm_i}})(\mathrm{P_{norm_i}})^{\mathrm{T}} \tag{12}$$

---

[14] Michael GREENACRE et al. “Principal component analysis”. In: *Nature Reviews Methods Primers* 2.1 (2022), p. 100.

[15] Hervé ABDI and Lynne J WILLIAMS. “Principal component analysis”. In: *Wiley interdisciplinary reviews: computational statistics* 2.4 (2010), pp. 433–459.

[16] G Thippa REDDY et al. “Analysis of dimensionality reduction techniques on big data”. In: *Ieee Access* 8 (2020), pp. 54776–54788.

Where N is the number of images. From the covariance matrix, the eigenvalues and eigenvectors are calculated using single value decomposition (SVD). The resulting eigenvalues show the amount of variance of each eigenvector, where higher values indicate components that capture a larger portion of the overall spread of the data. The eigen-vector matrix is then sorted from higher to lower eigenvalues, giving the matrix shown in equation 13.

$$\mathrm{W} = \begin{bmatrix} | & | & | \\ \mathrm{w}_1 & \mathrm{w}_2 & \mathrm{w}_\mathrm{k} \\ | & | & | \end{bmatrix}, \mathrm{w}_\mathrm{i} \in \mathrm{R}^\mathrm{M} \tag{13}$$

Where k is the number of principal components kept. The final reduced dataset is calculated using the operation shown in equation 14.

$$\hat{\mathrm{Y}} = \begin{bmatrix} \mathrm{w}_1^\mathrm{T} \mathrm{P}_{\mathrm{norm}_\mathrm{i}} \\ \mathrm{w}_2^\mathrm{T} \mathrm{P}_{\mathrm{norm}_\mathrm{i}} \\ \mathrm{w}_3^\mathrm{T} \mathrm{P}_{\mathrm{norm}_\mathrm{i}} \\ \vdots \\ \mathrm{w}_\mathrm{k}^\mathrm{T} \mathrm{P}_{\mathrm{norm}_\mathrm{i}} \end{bmatrix} \tag{14}$$

Given that $k < N$, the resultant dataset contains fewer images than the original dataset. This is a representation of the original data, projected onto a lower-dimensional space.

4. METHOD

This chapter describes the method used to generate calibration patterns, detailing each step from point spread function (PSF) generation through the compression process and PSF approximation using the designed calibration patterns. All the analysis was performed on a grayscale in order to study the spatial variations of the systems and also to match the implementation experiments where a grayscale camera was used through the acquisition process.

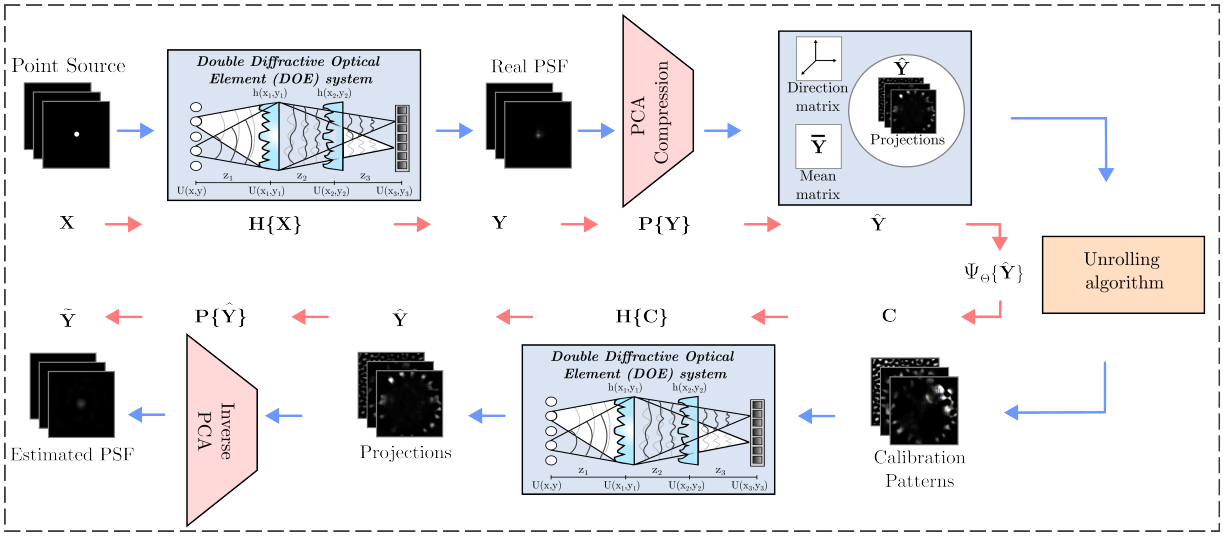

Figure 3. General flow diagram showing the different stages. The first step is to obtain the PSF of the optical system Y for later PCA compression in order to obtain $\hat{Y}$. An unrolling algorithm is used in order to obtain calibration patterns C. Once the calibration patterns are propagated through the optical system, the result is the projections $\hat{Y}$ and inverse PCA is used in order to obtain an approximation of the PSF $\tilde{Y}$

.

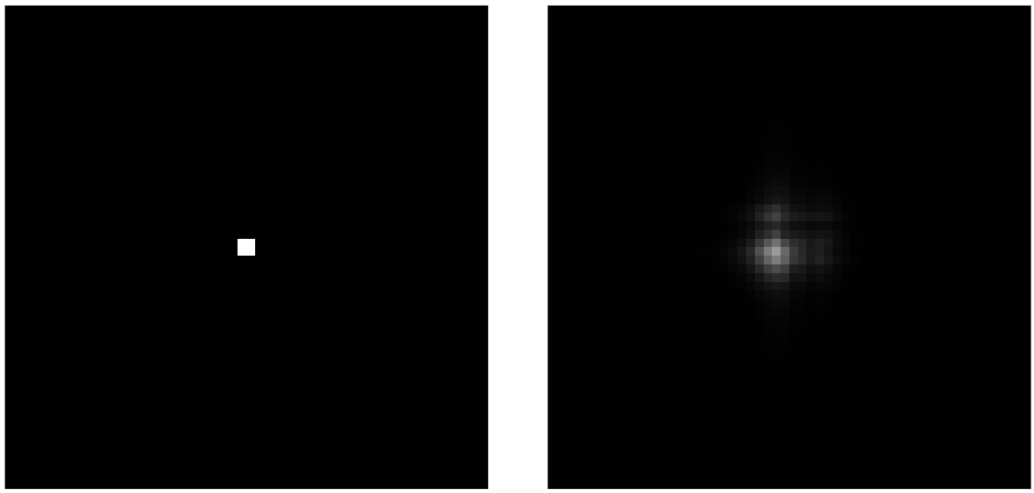

(a) Point Source (b) PSF

Figure 4. Comparison between Point source and generated PSF.

4.1. Point spread function dataset generation

Using the model from equations 4, 5, 6, the PSF at each spatial point of the selected image size was generated. For these generations, a set of images with a point source at different coordinates was generated. By propagating those images through the optical model, it is possible to generate the PSF at each pixel of the selected image size. Figure 4 shows the input image and the generated PSF at the same spatial point, and is possible to see that the system introduces a spatial variation to the input scene.

4.2. Calibration patterns

The PCA technique is used in this paper to obtain a representation of the principal components of the PSF dataset obtained previously. Each image was vectorized and stacked in a single MxN matrix, where M is the information of the images and N is the number of images. The result of this process were three 65536x65536 matrix, to which PCA was subsequently applied. Due to the computational intensity of PCA compres-

sion, only 11,000 projections were calculated from the 65,536 possible components, achieving the dataset reduction. During the PCA compression, the basis matrix representing the directions of maximum variance and the mean of the original data were stored. The projections obtained through PCA compression are reconstructed using an unrolling algorithm, which gives an approximation of the scene that, once propagated through the optical system, gives the PCA projections. Those reconstructions serve as the calibration patterns; figure 5 shows the original projection and its reconstruction using the unrolling algorithm respectively.

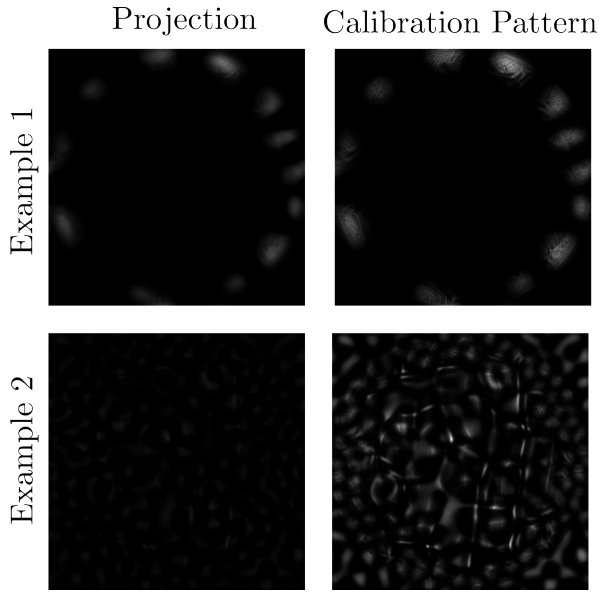

Figure 5. Comparison between projections $\hat{\mathbf{Y}}$ and calibration patterns $\mathbf{C}$, where its possible to see that the unrolling algorithm changes the intensity levels of the calibration patterns.

4.3. Reconstruction Process

The result of propagating the calibration patterns through the double DOE architecture, using the developed model, becomes the samples/features matrix for an inverse PCA calculation. These propagated calibration patterns are organized by vectorizing and stacking them vertically to form the samples/features matrix. Utilizing the basis matrix

containing the vectors of maximum variance and the mean of the original data enables the reconstruction process, following the calculation presented in Equation 15.

$$\tilde{\mathbf{Y}} = \mathbf{W}^{\mathbf{T}}\hat{\mathbf{Y}} + \bar{\mathbf{Y}} \tag{15}$$

Where $\bar{\mathbf{Y}}$ represents the mean of the original data and W denotes the basis matrix, both of which were stored during the PCA compression process. Each column of matrix $\tilde{\mathbf{Y}}$ corresponds to a PSF of the system. In this study, matrix $\tilde{\mathbf{Y}}$ has dimensions of 65,536 rows and 65,536 columns. By reshaping appropriately, it becomes possible to generate 65,536 images, each with a size of 256x256, representing the approximation of the PSF at each spatial point of the system.

5. OPTICAL IMPLEMENTATION

To evaluate the effectiveness of the designed method, the set of designed calibration patterns was captured using a real optical system. This system consisted of an objective lens, relay lens, beam splitter, deformable mirror (DM), DOE lens, and two cameras. The beam splitter was utilized to capture both the ground truth of the scene and the scene with the double DOE effect and the DM functioned as one of the DOEs in this configuration. Figure 6 shows the implemented system with all the optical elements mentioned before.

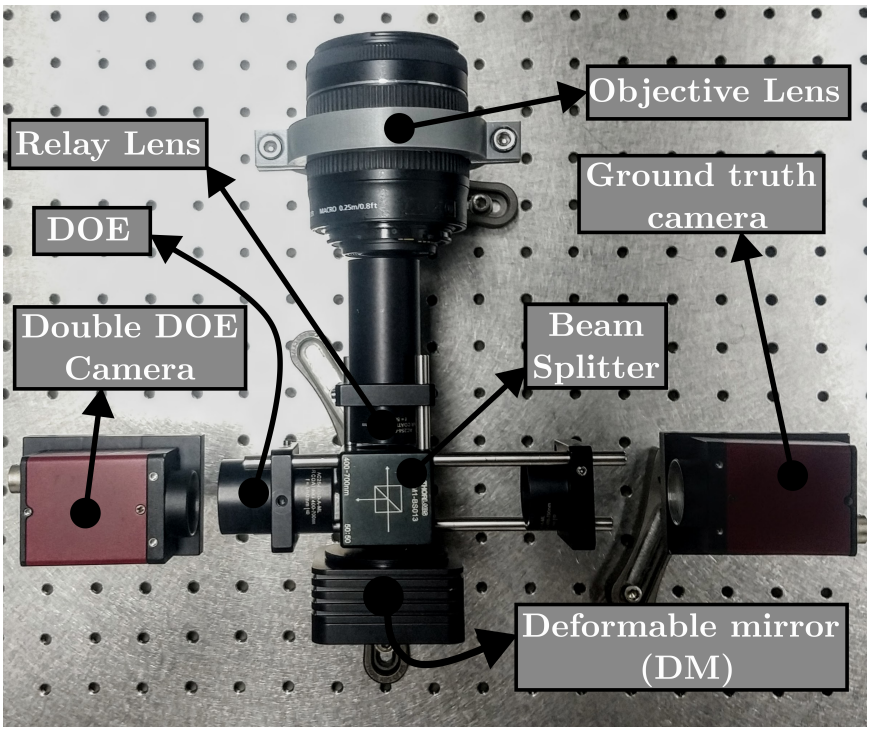

Figure 6. Double DOE optical system implementation.

Using the implemented system, a set of 1,500 calibration patterns and a set of 700 PSFs were acquired. Figs 7 illustrates the comparison between the ground truth using a calibration pattern as a scene and the calibration pattern acquired through the dou-

ble DOE system. Both ground truth and double DOE acquisition have a very similar structure with intensity differences. In figure 7 C, it is evident that the intensity of the acquired data is reduced due to the use of the beam splitter, which decreases the light intensity of the scene to $\frac{1}{4}$th of its original value. Later sections shows the results of the reconstructions using the acquired data.

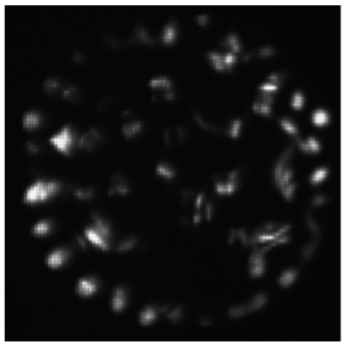

(a) Ground truth

(b) Double DOE acquisition

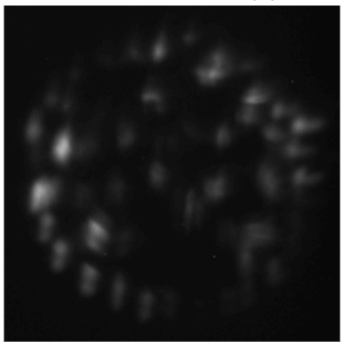

(c) Double DOE acquisition

Figure 7. Comparison between the ground truth and the acquired data through the double DOE. Figure C shows the double DOE acquisition with applied gamma correction just for visualization purposes.

Mathematically is possible to prove that, by acquiring the designed calibration patterns with a different double DOE system, the reconstructed PSF is an approximation of the PSF of the new system, the mathematical demonstration can be found in the GitHub repository. To prove this, first considering an optical system $\mathbf{H_1}$, and input scenes $\mathbf{X}$, equation 16 shows the result of propagating the scenes $\mathbf{X}$ through the system $\mathbf{H_1}$.

$$\mathbf{Y} = \mathbf{H_1 X} \tag{16}$$

Using a set of point sources as **X**, the resulting **Y** is the PSF of $\mathbf{H_1}$. Following the designed method, the complete PSF is compressed using PCA. Equation 17 shows the result of the PCA compression.

$$\hat{\mathbf{Y}} = \mathbf{WY} \tag{17}$$

Where **W** is the eigen-vector matrix of **Y** sorted from the highest to the lowest eigen-value. Assuming that $\mathbf{H_1}$ is completely invertible, the calibration patterns can be obtained by reversing the effect of the optical system as shown in equation 18.

$$\boldsymbol{C} = \mathbf{H_1^{-1}}\hat{\mathbf{Y}} \tag{18}$$

Equation 19 shows the replacement of equation 16 and 17 in equation 18.

$$\begin{aligned} \mathbf{C} &= \mathbf{H_1^{-1}WY} \\ \mathbf{C} &= \mathbf{H_1^{-1}WH_1X} \end{aligned} \tag{19}$$

Since the matrix W is non-defective and orthogonal, it follows that $\mathbf{WH_1} = \mathbf{H_1W}$. Equation 20 shows the simplified version of $\mathbf{C}$, where is visible that the calibration patterns do not depend of the optical system used.

$$\mathbf{C} = \mathbf{WX} \tag{20}$$

Considering another optical system $\mathbf{H_2}$, equation 21 shows the effect of the system over the designed calibration patterns **C**.

$$\hat{\mathbf{Y_2}} = \mathbf{H_2 C} \tag{21}$$

Equation 22 shows the replacement of equation 20 in equation 21.

$$\hat{\mathbf{Y_2}} = \mathbf{H_2 W X} \tag{22}$$

To reconstruct the PSF of H_2, an inverse PCA is performed. Equation 23 shows the result of the inverse PCA compression.

$$\mathbf{Y_2} = \mathbf{W^{-1}} \hat{\mathbf{Y_2}} \tag{23}$$

Equation 24 shows the replacement of the equation 22 in equation 23.

$$\mathbf{Y_2} = \mathbf{W^{-1} H_2 W X} \tag{24}$$

Since the matrix W is non-defective and orthogonal, it follows that $\mathbf{W H_2} = \mathbf{H_2 W}$. Equation 25 shows the simplified version of $\mathbf{Y_2}$, since $\mathbf{X}$ is a set of point sources, the product $\mathbf{H_2 X}$ or $\mathbf{Y_2}$ is the PSF of the system $\mathbf{H_2}$.

$$\mathbf{Y_2} = \mathbf{H_2 X} \tag{25}$$

One limitation of this analysis is its requirement for a full representation of the matrix $\mathbf{W}$, which in this specific case would be of size 65,536 by 65,536. To address this limitation, one can employ the first eigen-vectors of the matrix $\mathbf{W}$ for the inverse PCA process. This approach results in a reconstruction of the PSF along with an associated error value.

6. RESULTS

6.1. Simulation Results

The reconstruction process was tested using various numbers of calibration patterns. Figure 8 displays the average PSNR between the reconstruction and the generated PSF for each number of calibration patterns.

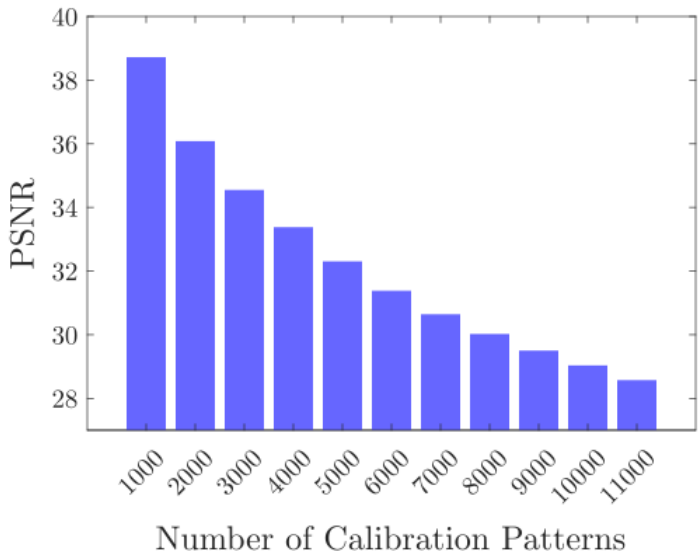

Figure 8. Average PSNR for different amounts of calibration patterns.

The behavior of the reconstruction graph demonstrate inconsistency with expected results, as the average PSNR should typically increase with the number of calibration patterns. Further investigation revealed intensity distortions in the reconstructed patterns caused by the unrolling algorithm. This algorithm accounts for the double DOE model during the reconstruction process. When applied to reconstruct an image that has not been propagated through this model, it introduces reconstruction errors, leading to altered intensities in the calibration patterns. This nonuniform intensity across all components resulted in a malfunction in the reconstruction process, with later com-

ponents having equal or greater influence than the initial ones. Figure 5 illustrate the differences between original and reconstructed projections from the top and bottom components, respectively; showing that the intensity of the propagated calibration patterns increases, distorting the original projection intensity. Consequently, fewer components result in better performance.

To test the accuracy of the method, a comparison between the reconstructed PSF and the generated PSF was conducted. Figure 9 displays the histogram of PSNR from the reconstruction using 1,000 and 11,000 calibration patterns. This histograms illustrate that the majority of reconstructions using 11000 calibration patterns exhibit a PSNR ranging from 25 to 40 [dB], which is considered to indicate high similarity. In Figure 8, is noticeable that the highest average PSNR is achieved when using 1,000 calibration patterns for the reconstruction process. This improvement is evident in Figure 9, which displays that most of the reconstructions exhibit PSNR values ranging from 37.5 [dB] to 45 [dB] compared to the generated PSF using the propagation model, representing an enhancement over the reconstruction using 11,000 components.

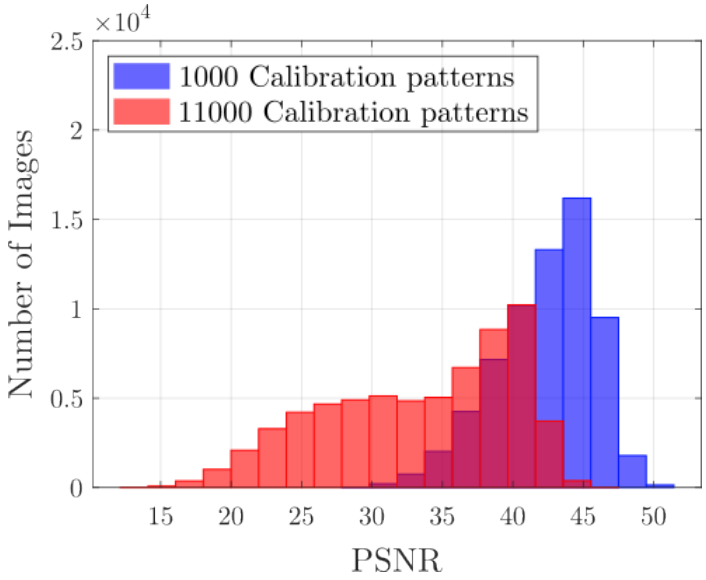

Figure 9. Comparison of PSNR histograms between reconstructed PSF and generated PSF using 1,000 and 11,000 calibration patterns.

To validate these results, the Structural Similarity Index (SSIM) metric was computed. Figure 10 presents the histograms of SSIM values between the reconstructed and original PSFs using 1,000 and 11,000 components for the reconstruction process. Comparing the patterns observed in figure 10, it is possible to see that most of the reconstructed images using less components display a similarity index from 60% to 100% compared to the original PSF, and by using 11,000 components the reconstructions process shows an uneven tendency with a considerable number of samples with an SSIM from 0 to 10%.

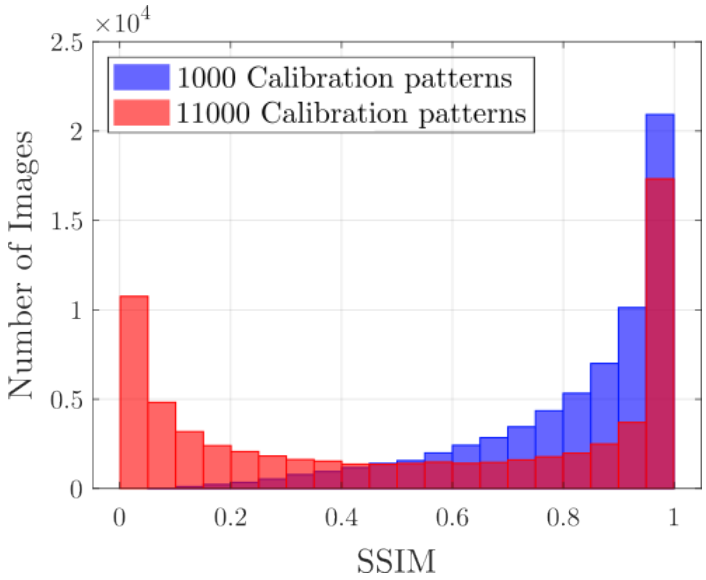

Figure 10. Comparison of SSIM histograms between reconstructed PSF and generated PSF using 1000 and 11,000 calibration patterns.

Furthermore, Figure 11 presents a comparison of the heat map illustrating the SSIM values between the reconstruction and the original PSF at each pixel. Figure 11 provides a clear illustration of the SSIM behavior using 11,000 components, showing inconsistencies across spatial points and indicating poor reconstruction quality. On the other hand, the reconstructions using 1,000 calibration patterns demonstrates more uniform values across all spatial points, indicating that reconstructions exhibit better similarities with fewer calibration patterns.

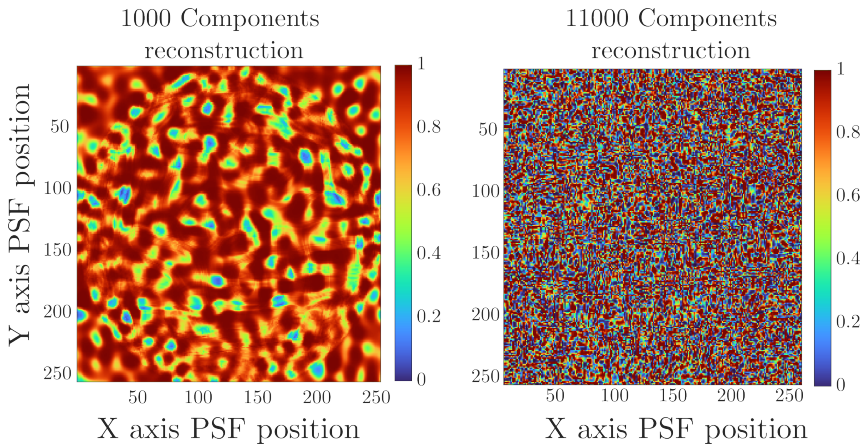

Figure 11. Comparison between heat maps representing the SSIM values between reconstructed PSF and generated PSF, across all the pixels of the simulation model.

6.2. Implementation results

The reconstruction process was performed using 1500 acquired components, and the resulting PSFs were compared to their corresponding acquired PSFs. Figure 12 shows the histograms for SSIM and PSNR values of the comparison between the acquired and reconstructed PSF. Figure 12 illustrates that the reconstructions exhibit SSIM values up to 65%, with an average value of 70%, which closely aligns with the simulation values. The disparity between the simulation and implementation values stems from the low light intensity in the captured calibration patterns, generated by the beam splitter employed in the implementation. This lack of intensity reduces the effectiveness of the reconstruction process. Figure 12 shows that the PSNR values go from 38 dB to 46 dB between reconstructed and acquired PSF, which represents a good reconstruction quality.

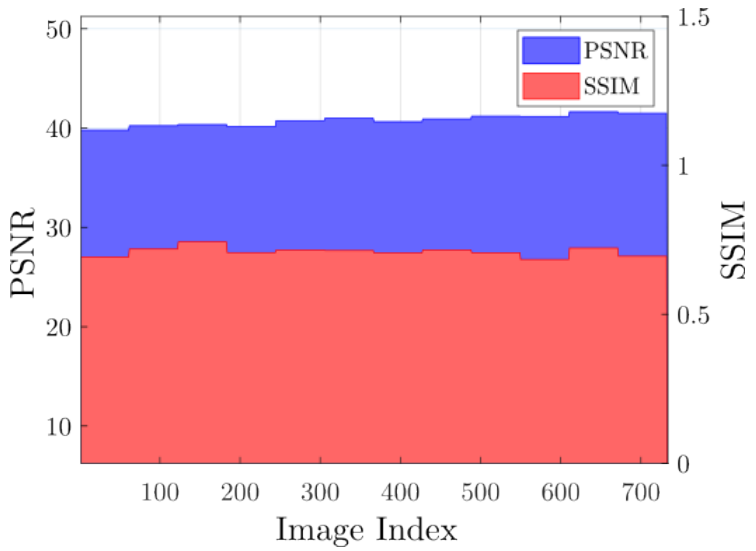

Figure 12. Comparison between acquired PSF and reconstructed PSF using 1,500 calibration patterns to the reconstruction process.

6.3. Conclusion

The proposed method and calibration patterns gave an accurate approximation of the PSF of the optical system used in the acquisition process, with PSNR values up to 40 dB and average SSIM 90% in simulation. Implementation results show that is possible to obtain a reconstruction of the PSF based on acquiring a set of calibration patterns with average PSNR, between acquired and reconstructed PSF, of 40 dB and average SSIM of 70%, requiring the acquisition of 1,000 to 11,000 calibration patterns which represents $\frac{1}{6}$th of the needed captures to acquire the PSF at each spatial point using a 256x256 image size. This leads to an improvement in tasks like CSI reconstruction, reversal of enconding, among others, as the PSF approximation can be calculated using a computational process instead of a time-consuming acquisition process. The optical implementation process had an exposure time of 10 seconds. With 1,500 calibration patterns acquired, the entire process took roughly 4 hours, which is significantly small compared to the 182 hours needed to acquire the complete PSF at each of the 65,536 pixels using the same exposure time. Mathematical procedures carried out during the

development of this research show that the designed calibration patterns can be used to obtain an approximation of the PSF of a different optical system from the one used to design them. The reconstruction process can be improved ensuring a good light intensity through the acquisition process and also, by using a better reconstruction algorithm that does not distort the intensity of the generated components through the PCA compression.

BIBLIOGRAPHY

ABDI, Hervé and Lynne J WILLIAMS. “Principal component analysis”. In: *Wiley interdisciplinary reviews: computational statistics* 2.4 (2010), pp. 433–459 (cit. on p. 19).

ALOUPOGIANNI, Eleni et al. “Design of a Hyper-Spectral Imaging System for Gross Pathology of Pigmented Skin Lesions”. In: *2021 43rd Annual International Conference of the IEEE Engineering in Medicine & Biology Society (EMBC)*. 2021, pp. 3605–3608. DOI: 10.1109/EMBC46164.2021.9629512 (cit. on p. 10).

ARGUELLO, Henry et al. “Shift-variant color-coded diffractive spectral imaging system”. In: *Optica* 8.11 (2021), pp. 1424–1434 (cit. on pp. 11, 14).

BACCA, Jorge, Emmanuel MARTINEZ, and Henry ARGUELLO. “Computational spectral imaging: a contemporary overview”. In: *J. Opt. Soc. Am. A* 40.4 (Apr. 2023), pp. C115–C125. DOI: 10.1364/JOSAA.482406 (cit. on pp. 10, 11).

BIASIO, Martin De et al. “UAV-based environmental monitoring using multi-spectral imaging”. In: *Airborne Intelligence, Surveillance, Reconnaissance (ISR) Systems and Applications VII*. Ed. by Daniel J. HENRY. Vol. 7668. International Society for Optics and Photonics. SPIE, 2010, p. 766811. DOI: 10.1117/12.864470 (cit. on p. 10).

DENIS, Loic et al. “Fast approximations of shift-variant blur”. In: *International Journal of Computer Vision* 115 (2015), pp. 253–278 (cit. on p. 14).

GE, Hongyi et al. “Applications of THz Spectral Imaging in the Detection of Agricultural Products”. In: *Photonics* 8.11 (2021). DOI: 10.3390/photonics8110518 (cit. on p. 10).

GOODMAN, Joseph W. *Introduction to Fourier optics*. Roberts and Company publishers, 2005 (cit. on p. 16).

GREENACRE, Michael et al. “Principal component analysis”. In: *Nature Reviews Methods Primers* 2.1 (2022), p. 100 (cit. on p. 19).

HU, Wei, Jianru XUE, and Nanning ZHENG. “PSF estimation via gradient domain correlation”. In: *IEEE Transactions on Image Processing* 21.1 (2011), pp. 386–392 (cit. on p. 12).

REDDY, G Thippa et al. “Analysis of dimensionality reduction techniques on big data”. In: *Ieee Access* 8 (2020), pp. 54776–54788 (cit. on p. 19).

REUTER, Alexander, Hans-Peter SEIDEL, and Ivo IHRKE. “BlurTags: spatially varying PSF estimation with out-of-focus patterns”. In: *20th International Conference on Computer Graphics, Visualization and Computer Vision 2012, WSCG’2012*. 2012, pp. 239–247 (cit. on p. 12).

ROBBINS, Gregory M and Thomas S HUANG. “Inverse filtering for linear shift-variant imaging systems”. In: *Proceedings of the IEEE* 60.7 (1972), pp. 862–872 (cit. on p. 14).

SHARMA, Nitika and Kriti SAROHA. “A novel dimensionality reduction method for cancer dataset using PCA and Feature Ranking”. In: *2015 International Conference on Advances in Computing, Communications and Informatics (ICACCI)*. 2015, pp. 2261–2264. DOI: 10.1109/ICACCI.2015.7275954 (cit. on p. 12).

STUART, Mary B., Andrew J. S. MCGONIGLE, and Jon R. WILLMOTT. “Hyperspectral Imaging in Environmental Monitoring: A Review of Recent Developments and Technological Advances in Compact Field Deployable Systems”. In: *Sensors* 19.14 (2019). DOI: 10.3390/s19143071 (cit. on p. 10).

URREA, Sergio et al. “Optical Solutions for Spectral Imaging Inverse Problems with a Shift-Variant System.” In: *Proceedings of the IEEE/CVF International Conference on Computer Vision*. 2023, pp. 4157–4164 (cit. on pp. 11, 15).